# Tuning the texture and polarity of ZnO thin films deposited by spatial atomic layer deposition through the addition of a volatile shape-directing agent

Chiara Crivello, Thomas Jalabert, Matthieu Weber, Hervé Roussel, Laetitia Rapenne, Hugo Mändar, Fabrice Donatini, Vincent Consonni, Gustavo Ardila, David Muñoz-Rojas

## Title

# Tuning the Texture and Polarity of ZnO Thin Films deposited by Spatial Atomic Layer Deposition through the Addition of a Volatile Shape-Directing Agent

Chiara Crivello [a], Thomas Jalaber [b], Matthieu Weber [a], Hervé Roussel [a], Laetitia Rapenne [a], Hugo Mädar [c], Fabrice Donatini [d], Vincent Consonni [a], Gustavo Ardila [b], David Muñoz-Rojas [a,*]

[a] Université Grenoble Alpes, CNRS, Grenoble INP, LMGP, Grenoble, France

[b] Université Grenoble Alpes, CNRS, Grenoble INP, IMEP-LaHC, F-38000 Grenoble, France

[c] Institute of Physic, University of Tartu,EE-50411 Tartu, Estonia

[d] Université Grenoble Alpes, CNRS, Grenoble INP, Institut NEEL, F-38000 Grenoble, France

*Corresponding author. E-mail: david.munoz-rojas@grenoble-inp.fr

### Highlights

- Use of a volatile shape directing agent to enhance the texture, growth rate, and piezoelectric coefficient of ZnO films deposited by spatial ALD
- The polarity of the ZnO films can be homogenized and switched with increasing concentration of volatile shape directing agent
- Original approach compatible with different substrates and conditions and high-throughput deposition

**TOC/Graphical Abstract**



## Abstract

Many functional devices are nowadays based on thin films deposited by physical or chemical vapour deposition methods. Being able to control the texture of the films is very important to tune their functional properties. Texture is commonly tuned by either using single crystalline substrates or seed layers, or by modifying the deposition parameters (gas flows, precursor concentration, temperature, etc.). In this study a volatile shape-directing agent (VSDA), namely 4-(5)-Methylimidazole (4-(5)-MeIM), is used during the deposition of ZnO thin films by Atmospheric-Pressure Spatial Atomic Layer Deposition (AP-SALD) to control the texture and growth rate of the films. In particular, ZnO thin films can be grown preferentially along (002), resulting in an enhanced piezoelectric coefficient. In addition, the polarity of the ZnO films also depends on the amount of VSDA used. An innovative industry-compatible approach to control texture and polarity of ZnO thin films is presented, having a clear potential for other functional materials and applications.



**Keywords** Piezoelectric ZnO films, textured thin films, atmospheric-pressure spatial atomic layer deposition, volatile shape-directing agent

## Introduction

Thin films are a ubiquitous component of functional devices such as sensors, solar cells, light-emitting diodes, functional coatings (antibacterial, self-cleaning…), etc. For some applications, the ability to control the texture of such thin films is of paramount importance to maximize their function properties (e.g. to optimize charge extraction in solar cells or to maximize catalytic efficiency). In most cases, functional thin films are deposited by physical or chemical vapour approaches, such as sputtering, chemical vapour deposition (CVD) or atomic layer deposition (ALD). However, controlling the texture of the deposited films by these approaches is not straightforward. Common approaches to tune film texture have been to use single-crystalline substrates, to introduce seed or buffer layers or to modify the deposition parameters. While these approaches are convenient to perform fundamental studies, they have limited industrial application since they either involve several fabrication steps or may require conditions not compatible with the manufactured device. It is therefore desirable to develop alternative methods allowing to control the texture of functional thin films and that are more compatible with mass production.

A material for which a control of the texture when growing it as a thin film is key to the resulting device properties is ZnO. ZnO has been largely studied since it can be easily deposited by many (low-cost) approaches, it has many applications (such as gas sensors, solar cells, thin-film transistors, and light-emitting diodes, [1–4]) and Zn is relatively abundant. In particular, ZnO crystallizes into the highly anisotropic wurtzite structure, making it piezoelectric. It is a biocompatible and non-critical material raising an increasing interest to replace already existing piezoelectric components made of toxic materials such as PZT. ZnO is also easy to integrate in a large variety of nanocomposites and substrates for electromechanical energy transduction applications such as energy harvesting [5] and sensing [6] or piezotronics applications where the electric transport in a transistor-like structure is controlled by the strain induced polarization [7]. Finally, it is also an intrinsic semiconductor. Thus, the competition between piezoelectricity, free charge carriers and surface traps permits the optimization of its piezoelectric properties, particularly in nanostructures [8].

The wurtzite structure is the most stable form of ZnO in normal ambient conditions, where $Zn^{2+}$ and $O^{2-}$ ions are distributed according to two interpenetrated hexagonal structures translated with respect to each other by the internal cell parameter *u*.[9] Generally, the $Zn^{2+}$ cation is coordinated by four $O^{2-}$ anions and *vice versa*, with tetrahedral coordination. This non-centrosymmetric structure, including the partially ionic bond of $Zn^{2+}$ and $O^{2-}$ ions, brings

to the formation of spontaneous piezoelectric polarization fields on the c-axis.[10,11] The formation of ZnO with irregular random crystal orientation causes a decrease of the piezoelectric output voltage, given that non-polar domains show no piezoelectric potential. In contrast, the semi-polar domains have a reduced piezoelectric potential [12].

In addition to piezoelectricity, the anisotropic nature of the wurzite makes ZnO polar. By convention, the [002] direction (*i.e.* +c-axis) is defined as the Zn polarity, while the opposite [00-2] direction (*i.e.* –c-axis) is defined as the O polarity [13]. It has been shown in the past two decades that polarity affects a large number of processes and properties in ZnO, including nucleation and growth mechanisms, defect incorporation and doping, electrical contacts or devices [14]. A striking example is given by the generation of a piezoelectric potential with an opposite sign in ZnO under mechanical solicitations and mixing O and Zn polarity domains, which can cancel out the output voltage in these piezoelectric devices [12]. The crystal polarity further plays a vital role during the nucleation and growth of ZnO, which can also affect its electrical and structural properties and its piezoelectric properties [4]. Accordingly, the growth of ZnO thin layers with a tunable and uniform polarity is of great significance for thin film-based devices, but also for nanowire-based devices where a polarity transfer occurs from the ZnO seed layer [15]. However, polarity is usually obtaining by depositing the ZnO thin films on buffer layers or ZnO single crystals. Tipically, the use of ZnO single crystals with either O or Zn polarity [16] or of buffer layers such as MgO [17], CrN [18], or $Cr_2O_3$ [19] has been reported to select the polarity of ZnO thin films. But the insertion of buffer layers in the stack can be detrimental for some physical properties. Alternatively, it would be highly desirable to find a way to tune or select the polarity of ZnO thin films during the growth process in order to preserve the stack.

ZnO thin films can be obtained by a large number of deposition methods, including solution ones, such as electrodeposition or the sol-gel approach, [20,21] or vapour deposition techniques, [22] such as sputtering, Molecular Beam Epitaxy (MBE) [19], Chemical Vapour Deposition (CVD) [23], or Atomic Layer Deposition (ALD) [24]. Of particular interest for industrial production and mass implementation, ZnO can easily be deposited by AP-SALD, a high-throughput deposition approach that is compatible with other in-line processes such as roll-to-roll [25,26]. SALD is a variant of ALD in which the precursors are injected continuously in separate regions of the reactor separated by an inert gas, thus eliminating the need for the purging step typical of ALD. As a result, SALD can be up to two orders of magnitude faster than ALD, even when processing at atmospheric pressure, reducing the cost of scaling up while keeping the good film properties [25,27,28]. Concerning the control of the

morphology of ZnO nanoparticles or the texture of ZnO thin films, this has been currently done in solution by using capping agents, i.e. small molecules that show different binding affinities different ZnO crystal facets [29–32]. Conversely, and as stated above, the control of texture of ZnO thin films deposited by vapour deposition approaches relies mostly on varying the deposition parameters or by modifying the substrate surface.

Inspired by the use of capping agents in solution approaches, we introduce here the use of a VSDA, namely 4-(5)-MeIM, and show that it can be used to tune the texture of ZnO thin films deposited by AP-SALD. The texture and piezoelectric properties of the films are a function of the amount of VSDA used. ZnO films oriented along (002) were obtained on glass and silicon, showing a maximum piezoelectric coefficient of 3.07 pm/V. In addition, we show that the presence of a VSDA also affects the polarity of the ZnO thin films deposited, which can be switched from mixture to Zn-polar to O-polar for increasing concentration of the VSDA. The switching of polarity is associated to an incorporation of N in the growing film as dopant. The present approach is expected to be valid for other materials and VSDAs and thus paves the way to new synthetic routes to control the properties of thin films deposited by vapour deposition methods.

## Experimental and Methods

The films were deposited using a home-made SALD system previously reported [33]. The system is based on a close-proximity injection head where the different flows carrying the metal precursor, co-reactant and inert gas are separated along parallel channels. The different precursors are place in bubblers that can be thermalized to increase the vapour pressure of the precursors. Then, by placing the substrate close enough to the deposition manifold, the separation between the precursors is achieved, having the gas-solid reactions on the substrate typical of ALD deposition.

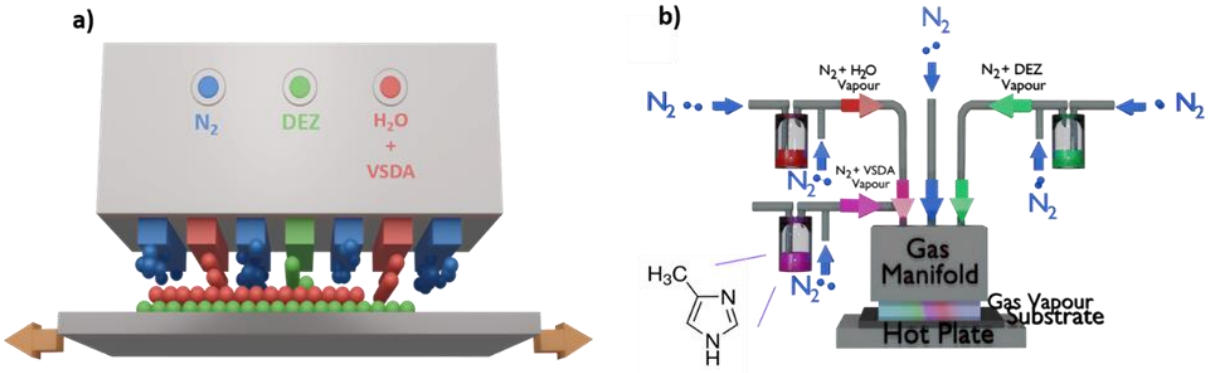


**Fig. 1 a** Schematic representation of the injection manifold with in blue the inert gas, in green is represented one precursor and in red the co-reactant. **b** Schematic representation of the AP-SALD close-proximity approach used for this work. The metallic precursor and the flow carrying it are represented in green. Red is used for water and purple is used for 4-(5)-Methylimidazole (VSDA). Blue is used for $N_2$

For the deposition of the ZnO films, Dyethilzinc (DEZ) from Strem Chemicals and deionized water were used. 4-(5)-Methylimidazole (4-(5)-MeIM) from Sigma Aldrich was used as VSDA. The bubbling and dilution flows for the three reactants was, respectively, 15/280, 50/225 and 100/100 sccm. Reference ZnO films were deposited using the following bubbling and dilution flows for DEZ and water: 30/270 and 150/300 sccm [34]. The nitrogen barrier flow was 500 sccm. The water and VSDA flows were mixed before reaching the head, and were injected at the same time through the same channels, as shown in Figure 1. The deposition temperature was in all cases 200 °C, and a distance between the injection manifold and the substrate of 150 µm was used. The number of ALD cycles was 600 for all samples. The substrate was scanned under the head at 180 mm/s. The bubbler containing the VSDA was heated at different temperatures (60, 70 and 80, the line being 5 °C hotter in all cases) to vary the concentration of VSDA in the flow. The samples were grown on silicon and glass substrates.

The surface morphology of the films was characterized by Scanning Electron Microscopy (SEM-FEG) with a Quanta 200 and a GeminiSEM 300 . Transmission Electron Microscopy (TEM) was performed with a JEOL JEM 2010 microscope operating at 200 kV, model INCA Energy TEM 100 X-Max 65 T, and $LaB_6$ as electron source. X-ray diffraction patterns were measured in a Bruker D8 Advance diffractometer in Bragg-Brentano (θ–2θ) configuration, with Cu Kα1 radiation (λ=0.15406 nm). X-ray reflectometry analysis (XRR) was performed

on a SmartLab$^{TM}$ (Rigaku) diffractometer using Cu Kα radiation (λ=0.154178 nm) from rotating anode X-ray tube working at 8.1 kW power. The program AXES was used for XRR pattern fitting and refinement. X-ray photoelectron spectroscopy (XPS) spectra were obtained with a ThermoScientific K-Alpha spectrometer using a monochromatized Al Kα radiation source (1486.6 eV), in ultra-high vacuum ($10^{-8}$ mbar) at room temperature. The X-Ray beam area (spot size) was adjusted to 400 µm in diameter. The peak analysis has been performed using the Avantage software. The samples were analysed without any etching step. The piezoelectric properties were examined using a Bruker Dimension Icon atomic force microscope (AFM) using the Contact Piezoresponse Force Miscroscopy (PFM) mode. An AC voltage modulation of 5 V was applied between the tip and the sample at a frequency in the range of 10-15 kHz chosen in order to avoid parasitic piezoelectric amplitude magnification. To reduce the electrostatic effect, which can affect the piezoelectric responses, a conductive tip (PtSi-NCH, Nanosensors) with a high spring constant (close to 43 N $m^{-1}$) was used for the PFM measurements. The 5 K cathodoluminescence spectroscopy was achieved with a FEI Inspect F50 FESEM instrument equipped with a liquid helium-cooled stage. The cathodoluminescence signal was collected on a 550 nm focal length monochromator equipped with a 600 grooves per mm diffraction grating with the help of a parabolic mirror. Cathodoluminscence spectra were acquired with a thermoelectric cooled silicon CCD detector.

## Results and Discussion

Figure 2 shows the SEM top-views and cross-sections of ZnO films deposited without VSDA and with the 4-(5)-MeIM heated at 60 °C, at 70 °C and 80 °C. The reference films present the typical morphology expected for ZnO (elongated grains). The approximate thickness of the films obtained after 600 ALD cycles was 96.2 nm, which corresponds to a GPC of 0.16 nm/cycle, in agreement with previous reports [35]. Conversely, the ZnO thin films obtained when using the VSDA present a different morphology, with grains that are rounder. Cross-section images show that, although the growth tends to be columnar in all cases, the thickness of the films increases with increasing amount of VSDA, thus implying that the addition of the 4-(5)-MeIM have an important impact on the process. XRR data also confirmed the impact of the addition of VSDA on the growth rate (see Figure S1).

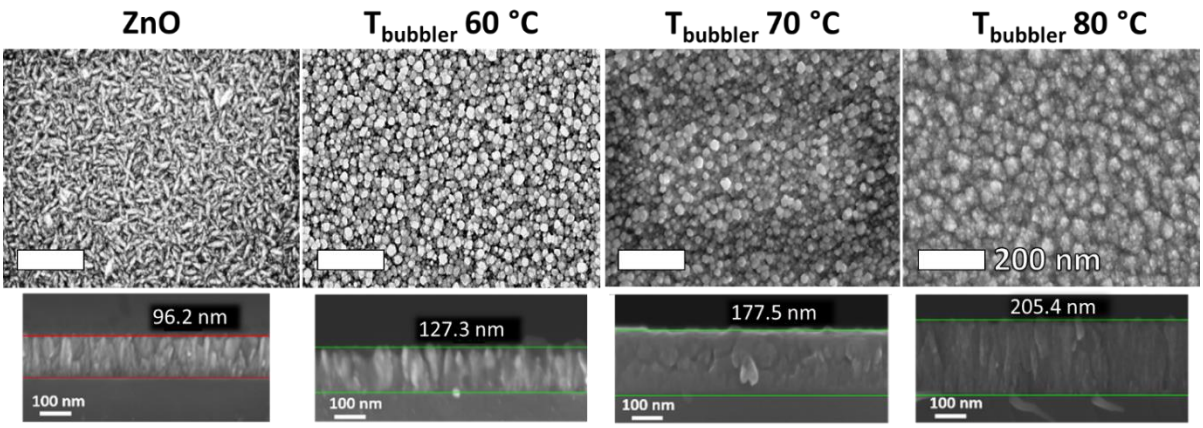


**Fig. 2** SEM images, from left to right of the ZnO by AP-SALD, and ZnO deposited by AP-SMLD with a $T_{bubbler}$ of 60 °C, 70 °C, and 80 °C, respectively. The first row is the top-view of the deposited samples, the second row is the cross-section of the same samples deposited on the silicon wafer. Measured approximate thickness values are indicated

XRD was used to evaluate the impact of the VSDA on the crystallinity of the films. The results, presented in Figure 3, show that the crystallinity is not very much affected by the presence or amount of VSDA. Conversely, a clear change in the texture of the films was observed when adding the VSDA. Reference ZnO films present four reflections: (100), 002, 101, and 110, the most intense one being the 002. By adding the organic compound, the film shows a preferential growth along the [002] direction, and the families of planes (100), (102), and (110) are slightly observed for the films deposited with the lowest amount of VSDA (precursor heated at 60 °C), while for the films deposited with higher amounts of VSDA these are not observed anymore. XRD results thus show that the addition of a VSDA affects both the growth rate and texture of the films.

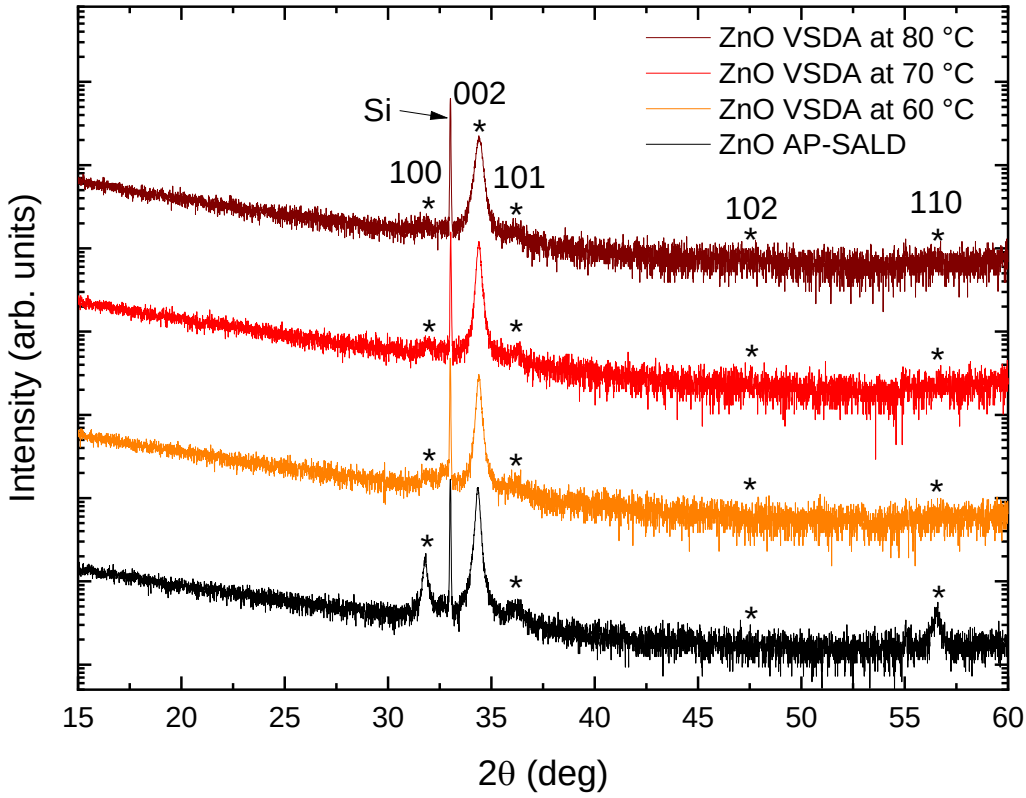


**Fig. 3** XRD patterns of ZnO thin films deposited without VSDA (black), with the VSDA heated at 60 °C (orange), at 70 °C (red), and 80 °C (bordeaux). The reflections marked with asterisk were identified belonging to ZnO phase (ICDD database card PDF-2 00-036-1451)

TEM analyses are presented in Figure 4 and confirm the results obtained by XRD. High-resolution TEM images show different families of planes and the columnar growth of the films. Selected-area electron diffraction (SAED) patters shows the diffraction spots from the Si substrate and dim diffraction rings along with more intense arcs that come from the ZnO films. The preferential orientation of the films along the [002] direction is reflected by the alignment of the more intense diffraction arcs with the Si substrate diffraction spot. An increasing degree of texture is observed with increasing amount of VSDA, as reflected by the decrease of the diffraction arc around the Si diffraction spot.

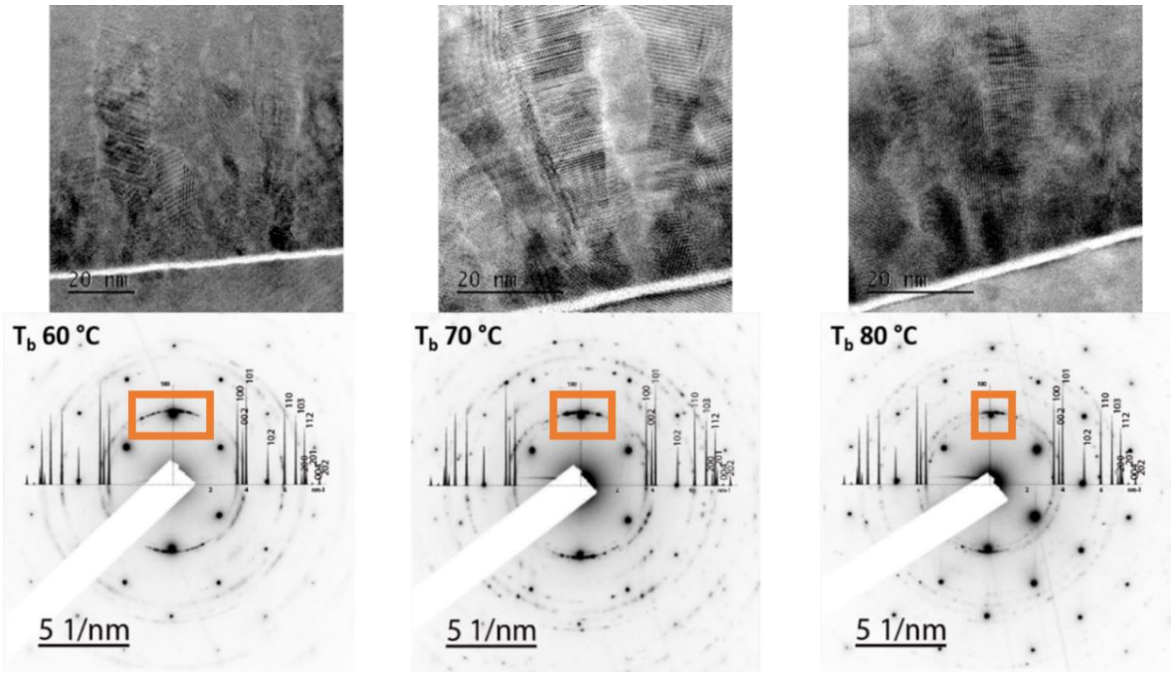


**Fig. 4** TEM images of the samples deposited on the silicon wafer with the organic compound at different temperatures. From left to right ($T_{bubbler}$ 60, 70, and 80 °C) with their relative electron diffraction patterns, which are taken on a large section of the samples, and are reported considering the Si diffraction pattern

From the above results, it can be concluded that the 4-(5)-MeIM molecules are interacting with the DEZ precursor in some manner during the deposition, which results in a preferential orientation of the films and an increased growth rate. Indeed, recent results have shown that organic molecules containing amine groups can form adducts with Zn metalorganic precursors [29], due to the affinity of N for Zn atoms [36]. This is confirmed by a study from Gandhi R. R. *et al.* [20], which proved that it is possible to control size and morphology of ZnO nanostructures using three different imidazole-based compounds in ionic assisted synthesis. Similarly, other studies have shown that imidazole-based molecules can be used as capping agents [37,38]. While these studies are performed in solution, we believe that similar interaction is to be expected in the gas phase. Indeed, this is confirmed by recent studies by R. Ameloot and co-workers involving the conversion of ZnO to MOF (metal-organic frameworks) by exposure if the former to vapours of imidazole based ligands. Indeed, the rate at which transformation occurs is highly dependent on the initial ZnO crystallinity and texture, which implies different binding affinities of the imidazole ligand to the different ZnO facets [39]. It is thus expected that during the deposition the imidazole molecules interact with

the Zn atoms in DEZ and with the ZnO particles being formed, which results in the enhanced deposition rate and texture evolution.

The texture obtained in crystalline thin films depends on different factors (temperature, metal source, solvent, etc.) [40–42]. In particular, conditions that provide different growth rates result in different textures [43], although the exact mechanism governing the obtained texture are not yet completely understood [30,41]. Zhang C. in 2010 proved that the nucleation process highly conditions the growth behaviour of the functional film material, in this particular case, by using a seed layer to grow the ZnO films [44]. On the other hand, the use of capping agents to control the morphology of nanostructures results in a thin layer of the capping agent attached to the surface of the nanostructures (in a core-shell fashion). Thus, if the texture evolution in the ZnO films presented here is the result of a capping effect by the imidazole molecules, one would expect to have imidazole molecules within the film. XPS was performed on the reference film and the textured films obtained with different amounts of VSDA to probe the presence of imidazole in the films. The results are presented in Figure S2 and show that no N is present in the reference film, as expected. Conversely, a weak, yet clear, N peak can be observed for the three samples deposited using the VSDA, depicting the presence of this element as traces (<1% atomic content; The stoechiometry of ZnO was not affected by the introduction of VSDA, as the Zn/O atomic ratio has been found to be 1 before and after the introduction of VSDA). The presence of N seems to indicate that the imidazole molecules bind to the growing ZnO and direct the texture, although more in-depth studies are necessary to elucidate the mechanisms taking place here.

As discussed above, a preferential orientation of ZnO films along the [002] direction is expected to enhance their piezoelectric response. To assess the impact on the piezoelectric properties of the films resulting from the texturing produced by the VSDA, PFM measurements were performed on our samples. Information on the direction of polarization is provided by the PFM phase [45]. As in the work by Bui Q. C. et al. [46], the origin of phases (+90°) is set so that Zn-polarity domains correspond to a positive phase (around 70°) whereas O-polarity domains correspond to a negative phase (around -80°). Figure 5 shows the PFM phase maps for the reference ZnO sample and the three samples obtained with VSDA heated at different temperature. The reference sample deposited without using the VSDA presents a large distribution of phases whereas the ones deposited with the VSDA have sharper distributions. In particular, the sample deposited with the highest amount of VSDA (bubbler heated at $80\,°C$) exhibit a narrow peak around -80°, corresponding to O polarity. In contrast, for lower concentrations of VSDA (bubbler heated at $60\,°C$ and 70 °C), the phase distribution

is broader and peaked around 30°, corresponding to a Zn polarity which is not perfectly vertically aligned. These results thus show that, quite remarkably, the addition of the VSDA agent during the deposition of ZnO results in both film texturing along [002] and the growth with a fixed polarity, which furthermore varies depending on the amount of VSDA used. Being able to control the texture and polarity of the ZnO films without the need of a buffer layer is very appealing for different applications, such as for energy harvesting applications [47,48].

The amplitude of the PFM signal is directly related to the piezoelectric coefficient of the material. We defined the effective piezoelectric coefficient $d_{33}^{eff}$ as the average PFM amplitude (See Figure S3 in the Supplementary Information) divided by the 5 V applied voltage modulation. A $d_{33}^{eff}$ coefficient of 1.97 $pm/V$ was extracted for the SALD sample, whereas $d_{33}^{eff}$ coefficients of 2.14 pm/V, 2.10 pm/V and 3.07 pm/V were extracted for the samples deposited with the VSDA heated at 60°C, 70°C and 80°C, respectively. Thus, the $d_{33}^{eff}$ coefficient measured on samples with Zn polarity (positive phases; VSDA heated at 60 and 70 °C) is smaller than the one measured on the sample with oxygen polarity (negative phases; VSDA heated at 80 °C). By contrast, in the work of Bui Q. C. et al. [46], a larger piezoelectric response amplitude was measured on ZnO thin films with Zn polarity as compared to ZnO thin films with O polarity. This can be explained by the better vertical alignment of the polar domains on the latter sample as demonstrated by the PFM phase values. Overall, the addition of the VSDA to the reaction and the resulting enhanced texture along [002] results in samples presenting higher piezoelectric responses compared to the reference ZnO sample.

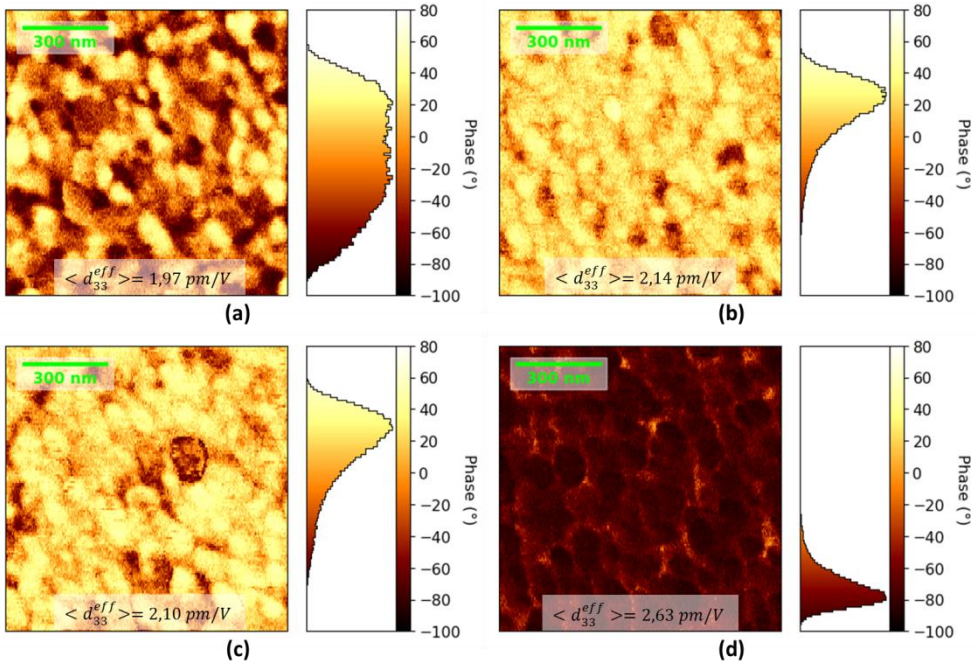

**Fig. 5** PFM acquisition of the samples to study the phase of the ZnO. **a** PFM acquisition of the sample ZnO AP-SALD with its relative phase distribution (i). **b** Acquisition of the sample of ZnO deposited with VSDA heated at 60 °C and it phase distribution. **c** Acquisition of the sample deposited with the VSDA heated at 70 °C and its phase distribution. **d** Acquisition of the sample deposited with the VSDA heated at 80 °C and its phase distribution

Considering that the VSDA is able to tune the texture and polarity of ZnO thin films, cathodoluminescence measurements were performed to investigate the crystalline quality, the nature and amount of defects incorporated as well as their dependence on the polarity. The 5 K cathodoluminescence spectra of ZnO thin films grown in AP-SALD standard conditions and using the 4-(5)-MeIM organic compound are presented in Figure 6. The near-band edge (NBE) emission of the standard ZnO thin film is dominated by the Y lines, namely the $Y_0$ and $Y_1$ lines pointing at 3.333 and 3.336 eV, respectively, which correspond to radiative transitions of excitons bound to structural defects [49]. These defects have been found to be located near the surfaces or at the vicinity of grain boundaries in ZnO thin films [50,51]. A shoulder at a higher energy shows the presence of radiative transitions involving free A-excitons ($FX_A$) and neutral donor bound A-excitons ($DX_A$). The radiative $FX_A$ transitions are located in the same range of energy for all the ZnO thin films, showing that their optical band gap energy does significantly vary. Following the *I* nomenclature used to label the excitonic lines [52], the $H_{BC}$, $I_6$,(Al) and $I_4$ ($H_O$) lines are expected to occur at 3.360, 3.3608, and 3.3628 eV, respectively [53]. This originates from residual contamination from the system as well as of hydrogen from the chemical precursors used by AP-SALD [54]. Correlatively, a weak shoulder at a lower energy involves the corresponding two electron satellites (TES) lines associated with the $H_{BC}$, $I_6$,(Al) and $I_4$ ($H_O$) lines in the range of 3.32-3.33 eV. Notably, the visible band emission centred at around 2.1 eV exhibits a much lower intensity and is very broad. Interestingly, the use of the 4-(5)-MeIM organic compound heated at 60 and 70 °C during the AP-SALD process causes a significant variation of the 5 K cathodoluminescence spectra of Zn-polar ZnO thin films. The intensity of the NBE emission is strongly reduced, while the visible band emission remains unaffected in terms of both shape and intensity. More importantly, although the Y lines as well as the $FX_A$, $DX_A$ and TES lines still occur, the NBE emission is dominated by a broad band centred at around 3.29 eV, which can be assigned to donor-acceptor pair (DAP) and free-electron-to-acceptor (FA) transitions involving nitrogen acting as an acceptor in ZnO [55,56]. The bulk incorporation of nitrogen prevails in Zn-polar ZnO thin films, which is in agreement with [57]. Eventually, the use of the 4-(5)-MeIM

organic compound heated at 80 °C during the AP-SALD process causes an even stronger variation of the 5 K cathodoluminescence spectrum of the O-polar ZnO thin film. The intensity of the NBE emission is drastically increased, while the visible band emission remains again unaffected in terms of both shape and intensity. This indicates a much better crystallinity of O-polar ZnO thin film. The NBE emission is again dominated by the Y lines, while the $FX_A$, $DX_A$, and TES lines occur. The shoulder at a lower energy still indicates the occurrence of DAP and FA transitions involving nitrogen but with a much lower intensity. It is thus expected here that a less pronounced incorporation of nitrogen occurs in O-polar ZnO thin film than in Zn-polar ZnO thin films, which is in agreement with [57]. Cathodoluminescence spectra thus confirm the incorporation of N in the films and agree with the evolution of the polarity of the films with respect to the amount of VSDA used. Interestingly, the higher crystalline quality of O-polar ZnO thin films along with a better alignment along the *c*-axis certainly prevails to increae the piezoelectric response amplitude measured by PFM, despite the small incorporation of nitrogen. However, the implication of N related defect complexes might play a significant role as well. Nitrogen is known to substitute for O atoms ($N_O$) in ZnO, but also to favour the formation of defect complexes including $N_O$-H [58] and $V_{Zn}$-$N_O$-H with a low formation energy and acting as a deep acceptor [59]. In the present case, the effect of the improvement of the structural properties dominates the effect of the differential incorporation of nitrogen to generally increase the piezoelectric response amplitude in O-polar ZnO thin films.

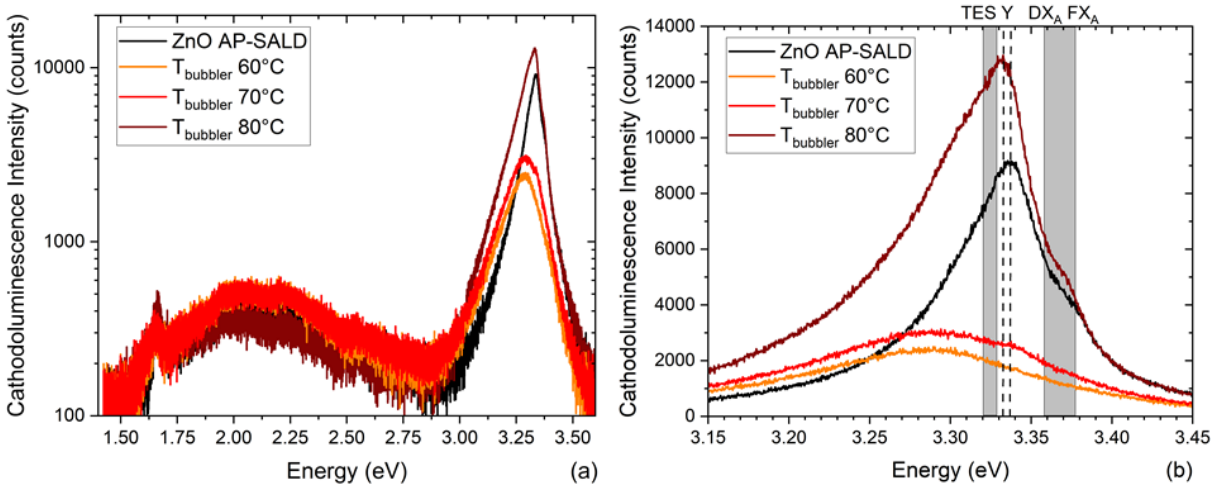


**Fig. 6** 5K cathodoluminescence spectra of ZnO deposited in AP-SALD standard conditions (black) and with the organic compound 4-(5)-MeIM heated at 60 °C (orange), at 70 °C (red), and 80 °C (burgundy). To plot the patterns a logarithmic scale was used

## Conclusions

While the use of capping agents have been extensively achieved in solution/based synthetic approached to control the size and morphology of nanostructures and the texture of deposited films, the control of texture in gas-based deposition approaches has mostly relied on a variation of the deposition parameters and/or the use of single crystalline substrates or buffer/seed layers. In this work, we demonstrate that VSDA can be used to control the texture of films deposited by gas-based deposition methods. In particular, the texture of ZnO films deposited by AP-SALD has been modified by adding a volatile imidazole based molecule, namely 4-(5)-MeIM. ZnO thin films deposited in the presence of the VSDA show an enhanced texture along [002] direction. We also show that the addition of the VSDA to the reaction has a strong impact on the deposition rate and, most remarkably, the polarity of the ZnO films obtained. Thus, increasing the amounts of VSDA results in faster deposition rates and a polarity evolution from random to Zn-polar (VSDA heated at 60 and 70° C) to O-polar (VSDA at 80 °C). The interaction between the VSDA and the forming ZnO particles leads to an incorporation of N in the films, as evidenced by XPS and 5 K cathodoluminescence easurements. The enhanced texture results in an increase of the piezoelectric coefficient $d_{33}^{eff}$ from 1.97 to 3.07 pm/V. Our findings report a new way to tune the texture and polarity of films deposited by CVD and other gas-based deposition approaches, which will provide an extra degree of freedom for the design of functional materials and devices.

## Acknowledgments

D.M.-R. acknowledges support from from the FETOPEN-1-2016-2017 research and innovation program under Grant Agreement 801464 (SPRINT). The authors acknowledge the CMTC characterization platform of Grenoble INP (Institute of Engineering) supported by the Centre of Excellence of Multifunctional Architectured Materials “CEMAM” n°ANR-10-LABX-44-01 funded by the “Investments for the Future” Program. This work has been partly supported by the project PULSE-COM of the European Union’s Horizon 2020 research and innovation programme under grant agreement No 863227. H.M. Acknowledges funding throught he European Regional Development Fund project TK134 “Emerging orders in quantum and nanomaterials” .H.M., C.C. and D.M.R. acknowledge support from the ministère de l'Europe et des Affaires étrangères (MEAE), the ministère de l'Enseignement

supérieur, de la Recherche et de l'Innovation (MESRI) and the Estonian Research Council (ETAG) through the Parrot program.

## Data Availability

The raw data required to reproduce these findings are available upon request to the corresponding author. The processed data required to reproduce these findings are available upon request to the corresponding author.

## References

[1] M.-J. Zhao, Z.-T. Sun, C.-H. Hsu, P.-H. Huang, X.-Y. Zhang, W.-Y. Wu, P. Gao, Y. Qiu, S.-Y. Lien, W.-Z. Zhu, Zinc Oxide Films with High Transparency and Crystallinity Prepared by a Low Temperature Spatial Atomic Layer Deposition Process, Nanomaterials. **10**, 459 (2020). https://doi.org/10.3390/nano10030459.

[2] J. Dong, D. Han, H. Li, W. Yu, S. Zhang, X. Zhang, Y. Wang, Effect of Al doping on performance of ZnO thin film transistors, Appl. Surf. Sci. **433**, 836 (2018). https://doi.org/10.1016/j.apsusc.2017.10.071.

[3] A. Verbič, M. Gorjanc, B. Simončič, Zinc Oxide for Functional Textile Coatings: Recent Advances, Coatings. **9**, 550 (2019). https://doi.org/10.3390/coatings9090550.

[4] Z.L. Wang, From nanogenerators to piezotronics—A decade-long study of ZnO nanostructures, MRS Bull. **37**, 814 (2012). https://doi.org/10.1557/mrs.2012.186.

[5] R. Tao, M. Parmar, G. Ardila, P. Oliveira, D. Marques, L. Montès, M. Mouis, Performance of ZnO based piezo-generators under controlled compression, Semicond. Sci. Technol. **32**, 064003 (2017). https://doi.org/10.1088/1361-6641/aa691f.

[6] M. Parmar, E.A.A. Leon Perez, G. Ardila, E. Saoutieff, E. Pauliac-Vaujour, M. Mouis, A demonstration of the mechanical sensing capability of individually contacted vertical piezoelectric nanowires arranged in matrices, Nano Energy. **56**, 859 (2019). https://doi.org/10.1016/j.nanoen.2018.11.088.

[7] Y. Zhang, Y. Liu, Z.L. Wang, Fundamental Theory of Piezotronics, Adv. Mater. **23**, 3004 (2011). https://doi.org/10.1002/adma.201100906.

[8] A.J.L. Lopez Garcia, M. Mouis, V. Consonni, G. Ardila, Dimensional Roadmap for

Maximizing the Piezoelectrical Response of ZnO Nanowire-Based Transducers: Impact of Growth Method, Nanomaterials. **11**, 941 (2021). https://doi.org/10.3390/nano11040941.

[9] Z.L. Wang, Zinc oxide nanostructures: growth, properties and applications, J. Phys. Condens. Matter. **16**, R829 (2004). https://doi.org/10.1088/0953-8984/16/25/R01.

[10] A. Janotti, C.G. Van de Walle, Fundamentals of zinc oxide as a semiconductor, Reports Prog. Phys. **72**, 126501 (2009). https://doi.org/10.1088/0034-4885/72/12/126501.

[11] A. Kołodziejczak-Radzimska, T. Jesionowski, Zinc Oxide—From Synthesis to Application: A Review, Materials (Basel). **7**, 2833 (2014). https://doi.org/10.3390/ma7042833.

[12] J.G.E. Gardeniers, Z.M. Rittersma, G.J. Burger, Preferred orientation and piezoelectricity in sputtered ZnO films, J. Appl. Phys. **83**, 7844 (1998). https://doi.org/10.1063/1.367959.

[13] J. Goniakowski, F. Finocchi, C. Noguera, Polarity of oxide surfaces and nanostructures, Reports Prog. Phys. **71**, 016501 (2008). https://doi.org/10.1088/0034-4885/71/1/016501.

[14] J. Zúñiga-Pérez, V. Consonni, L. Lymperakis, X. Kong, A. Trampert, S. Fernández-Garrido, O. Brandt, H. Renevier, S. Keller, K. Hestroffer, M.R. Wagner, J.S. Reparaz, F. Akyol, S. Rajan, S. Rennesson, T. Palacios, G. Feuillet, Polarity in GaN and ZnO: Theory, measurement, growth, and devices, Appl. Phys. Rev. **3**, 041303 (2016). https://doi.org/10.1063/1.4963919.

[15] V. Consonni, A.M. Lord, Polarity in ZnO nanowires: A critical issue for piezotronic and piezoelectric devices, Nano Energy. **83**, 105789 (2021). https://doi.org/10.1016/j.nanoen.2021.105789.

[16] S. Lautenschlaeger, J. Sann, N. Volbers, B.K. Meyer, A. Hoffmann, U. Haboeck, M.R. Wagner, Asymmetry in the excitonic recombinations and impurity incorporation of the two polar faces of homoepitaxially grown ZnO films, Phys. Rev. B. **77**, 144108 (2008). https://doi.org/10.1103/PhysRevB.77.144108.

[17] H. Kato, K. Miyamoto, M. Sano, T. Yao, Polarity control of ZnO on sapphire by varying the MgO buffer layer thickness, Appl. Phys. Lett. **84**, 4562 (2004).

https://doi.org/10.1063/1.1759377.

[18] J.S. Park, S.K. Hong, T. Minegishi, S.H. Park, I.H. Im, T. Hanada, M.W. Cho, T. Yao, J.W. Lee, J.Y. Lee, Polarity control of ZnO films on (0001) Al2O3 by Cr-compound intermediate layers, Appl. Phys. Lett. **90**, 201907 (2007). https://doi.org/10.1063/1.2740190.

[19] J.S. Park, J.H. Chang, T. Minegishi, H.J. Lee, S.H. Park, I.H. Im, T. Hanada, S.K. Hong, M.W. Cho, T. Yao, Growth of Polarity-Controlled ZnO Films on (0001) Al2O3, J. Electron. Mater. **37**, 736 (2008). https://doi.org/10.1007/s11664-007-0350-y.

[20] R. Rajiv Gandhi, S. Gowri, J. Suresh, M. Sundrarajan, Ionic Liquids Assisted Synthesis of ZnO Nanostructures: Controlled Size, Morphology and Antibacterial Properties, J. Mater. Sci. Technol. **29**, 533 (2013). https://doi.org/10.1016/j.jmst.2013.03.007.

[21] H. Makhlouf, M. Weber, O. Messaoudi, S. Tingry, M. Moret, O. Briot, R. Chtoutou, M. Bechelany, Study of Cu 2 O\ZnO nanowires heterojunction designed by combining electrodeposition and atomic layer deposition, Appl. Surf. Sci. **426**, 301 (2017). https://doi.org/10.1016/j.apsusc.2017.07.130.

[22] E. Przezdziecka, E. Guziewicz, D. Jarosz, D. Snigurenko, A. Sulich, P. Sybilski, R. Jakiela, W. Paszkowicz, Influence of oxygen-rich and zinc-rich conditions on donor and acceptor states and conductivity mechanism of ZnO films grown by ALD—Experimental studies, J. Appl. Phys. **127**, 075104 (2020). https://doi.org/10.1063/1.5120355.

[23] S. Chen, J. Wang, Z. Zhang, J. Briscoe, M.E.A. Warwick, H. Li, P. Hu, Aerosol assisted chemical vapour deposition of conformal ZnO compact layers for efficient electron transport in perovskite solar cells, Mater. Lett. **217**, 251 (2018). https://doi.org/10.1016/j.matlet.2018.01.090.

[24] T. Tynell, M. Karppinen, Atomic layer deposition of ZnO: a review, Semicond. Sci. Technol. **29**, 043001 (2014). https://doi.org/10.1088/0268-1242/29/4/043001.

[25] P. Poodt, D.C. Cameron, E. Dickey, S.M. George, V. Kuznetsov, G.N. Parsons, F. Roozeboom, G. Sundaram, A. Vermeer, Spatial atomic layer deposition: A route towards further industrialization of atomic layer deposition, J. Vac. Sci. Technol. A Vacuum, Surfaces, Film. **30**, 010802 (2012). https://doi.org/10.1116/1.3670745.

[26] K.P. Musselman, C.F. Uzoma, M.S. Miller, Nanomanufacturing: High-Throughput, Cost-Effective Deposition of Atomic Scale Thin Films via Atmospheric Pressure Spatial Atomic Layer Deposition, Chem. Mater. **28**, 8443 (2016). https://doi.org/10.1021/acs.chemmater.6b03077.

[27] D. Muñoz-Rojas, T. Maindron, A. Esteve, F. Piallat, J.C.S. Kools, J.-M. Decams, Speeding up the unique assets of atomic layer deposition, Mater. Today Chem. **12**, 96 (2019). https://doi.org/10.1016/j.mtchem.2018.11.013.

[28] A. Sekkat, M.O. Liedke, V.H. Nguyen, M. Butterling, F. Baiutti, J. de D. Sirvent Veru, M. Weber, L. Rapenne, D. Bellet, G. Chichignoud, A. Kaminski-Cachopo, E. Hirschmann, A. Wagner, D. Muñoz-Rojas, Chemical deposition of Cu2O films with ultra-low resistivity: correlation with the defect landscape, Nat. Commun. **13**, 5322 (2022). https://doi.org/10.1038/s41467-022-32943-4.

[29] Y. Wang, Y. Coppel, C. Lepetit, J.-D. Marty, C. Mingotaud, M. Kahn, Anisotropic Growth of ZnO Nanoparticles Driven by the Structure of Amine Surfactants: The Surface Dynamic on Nanocrystal Rules, Nanoscale Adv. (2021). https://doi.org/10.1039/d1na00566a.

[30] K. Biswas, B. Das, C.N.R. Rao, Trends in Chemistry of Materials: Selected Research Papers of CNR Rao, World Scientific, 2008.

[31] P. Basnet, S. Chatterjee, Structure-directing property and growth mechanism induced by capping agents in nanostructured ZnO during hydrothermal synthesis—A systematic review, Nano-Structures & Nano-Objects. **22**, 100426 (2020). https://doi.org/https://doi.org/10.1016/j.nanoso.2020.100426.

[32] X. Ren, W. Dang, Q. Ma, X. Zhu, W. Zi, L. Jia, B. Liu, X. Zhang, F. Xiao, H. Yang, Z. Yang, S. (Frank) Liu, Superior texture-controlled ZnO thin film using electrochemical deposition, Sol. Energy. **125**, 192 (2016). https://doi.org/10.1016/j.solener.2015.12.018.

[33] D. Muñoz-Rojas, V.H. Nguyen, C. Masse de la Huerta, S. Aghazadehchors, C. Jiménez, D. Bellet, Spatial Atomic Layer Deposition (SALD), an emerging tool for energy materials. Application to new-generation photovoltaic devices and transparent conductive materials, Comptes Rendus Phys. **18**, 391 (2017). https://doi.org/10.1016/j.crhy.2017.09.004.

[34] V.H. Nguyen, D. Bellet, B. Masenelli, D. Muñoz-Rojas, Increasing the Electron Mobility of ZnO-Based Transparent Conductive Films Deposited by Open-Air Methods for Enhanced Sensing Performance, ACS Appl. Nano Mater. **1**, 6922 (2018). https://doi.org/10.1021/acsanm.8b01745.

[35] R.L.Z. Hoye, D. Muñoz-Rojas, S.F. Nelson, A. Illiberi, P. Poodt, F. Roozeboom, J.L. Macmanus-Driscoll, Research Update: Atmospheric pressure spatial atomic layer deposition of ZnO thin films: Reactors, doping, and devices, APL Mater. **3**, (2015). https://doi.org/10.1063/1.4916525.

[36] J. Jayabharathi, M. Sundharesan, A. Prabhakaran, C. Karunakaran, Understanding the binding interaction of imidazole with ZnO nanomaterials and clusters, RSC Adv. **5**, 9518 (2015). https://doi.org/10.1039/C4RA15957H.

[37] J. Mishra, M. Jha, N. Kaur, A.K. Ganguli, Room temperature synthesis of urea based imidazole functionalised ZnO nanorods and their photocatalytic application, Mater. Res. Bull. **102**, 311 (2018). https://doi.org/10.1016/j.materresbull.2018.02.045.

[38] A.K. Padhy, B. Chetia, S. Mishra, A. Pati, P.K. Iyer, Imidazole derivatives as the organic precursor of ZnO nano particle, Tetrahedron Lett. **51**, 2751 (2010). https://doi.org/https://doi.org/10.1016/j.tetlet.2010.03.058.

[39] T. Stassin, I. Stassen, N. Wauteraerts, A.J. Cruz, M. Kräuter, A.M. Coclite, D. De Vos, R. Ameloot, Solvent-Free Powder Synthesis and Thin Film Chemical Vapor Deposition of a Zinc Bipyridyl-Triazolate Framework, Eur. J. Inorg. Chem. 71 (2020). https://doi.org/https://doi.org/10.1002/ejic.201901051.

[40] G. Yergaliuly, B. Soltabayev, S. Kalybekkyzy, Z. Bakenov, A. Mentbayeva, Effect of thickness and reaction media on properties of ZnO thin films by SILAR, Sci. Rep. **12**, 851 (2022). https://doi.org/10.1038/s41598-022-04782-2.

[41] I. Petrov, P.B. Barna, L. Hultman, J.E. Greene, Microstructural evolution during film growth, J. Vac. Sci. \& Technol. A. **21**, S117 (2003). https://doi.org/10.1116/1.1601610.

[42] S. Arya, P. Mahajan, S. Mahajan, A. Khosla, R. Datt, V. Gupta, S.-J. Young, S.K. Oruganti, Review—Influence of Processing Parameters to Control Morphology and Optical Properties of Sol-Gel Synthesized ZnO Nanoparticles, ECS J. Solid State Sci. Technol. **10**, 23002 (2021). https://doi.org/10.1149/2162-8777/abe095.

[43] H. Liu, V.H. Nguyen, H. Roussel, I. Gélard, L. Rapenne, J.-L. Deschanvres, C. Jiménez, D. Muñoz-Rojas, The Role of Humidity in Tuning the Texture and Electrical Properties of Cu2O Thin Films Deposited via Aerosol-Assisted CVD, Adv. Mater. Interfaces. **6**, 1801364 (2019). https://doi.org/https://doi.org/10.1002/admi.201801364.

[44] C. Zhang, High-quality oriented ZnO films grown by sol–gel process assisted with ZnO seed layer, J. Phys. Chem. Solids. **71**, 364 (2010). https://doi.org/10.1016/j.jpcs.2010.01.001.

[45] A. Gruverman, M. Alexe, D. Meier, Piezoresponse force microscopy and nanoferroic phenomena, Nat. Commun. **10**, 1661 (2019). https://doi.org/10.1038/s41467-019-09650-8.

[46] Q.C. Bui, G. Ardila, H. Roussel, C. Jiménez, I. Gélard, O. Chaix-Pluchery, X. Mescot, S. Boubenia, B. Salem, V. Consonni, Tuneable polarity and enhanced piezoelectric response of ZnO thin films grown by metal–organic chemical vapour deposition through the flow rate adjustment, Mater. Adv. **3**, 498 (2022). https://doi.org/10.1039/D1MA00921D.

[47] W. Rahman, S. Garain, A. Sultana, T. Ranjan Middya, D. Mandal, Self-Powered Piezoelectric Nanogenerator Based on Wurtzite ZnO Nanoparticles for Energy Harvesting Application, in: Mater. Today Proc., 2018: pp. 9826–9830. www.sciencedirect.comwww.materialstoday.com/proceedings (accessed November 29, 2021).

[48] A.T. Le, M. Ahmadipour, S.-Y. Pung, A review on ZnO-based piezoelectric nanogenerators: Synthesis, characterization techniques, performance enhancement and applications, J. Alloys Compd. **844**, 156172 (2020). https://doi.org/10.1016/j.jallcom.2020.156172.

[49] C. Morhain, M. Teisseire, S. Vézian, F. Vigué, F. Raymond, P. Lorenzini, J. Guion, G. Neu, J.-P. Faurie, Spectroscopy of Excitons, Bound Excitons and Impurities in h-ZnO Epilayers, Phys. Status Solidi. **229**, 881 (2002). https://doi.org/https://doi.org/10.1002/1521-3951(200201)229:2<881::AID-PSSB881>3.0.CO;2-3.

[50] V.S. Yalishev, Y.S. Kim, X.L. Deng, B.H. Park, S.U. Yuldashev, Study of the photoluminescence emission line at 3.33 eV in ZnO films, J. Appl. Phys. **112**, 13528

(2012). https://doi.org/10.1063/1.4733952.

[51] S. Guillemin, V. Consonni, L. Rapenne, E. Sarigiannidou, F. Donatini, G. Bremond, Identification of extended defect and interface related luminescence lines in polycrystalline ZnO thin films grown by sol–gel process, RSC Adv. **6**, 44987 (2016). https://doi.org/10.1039/C6RA04634G.

[52] B.K. Meyer, H. Alves, D.M. Hofmann, W. Kriegseis, D. Forster, F. Bertram, J. Christen, A. Hoffmann, M. Straßburg, M. Dworzak, U. Haboeck, A. V Rodina, Bound exciton and donor–acceptor pair recombinations in ZnO, Phys. Status Solidi. **241**, 231 (2004). https://doi.org/https://doi.org/10.1002/pssb.200301962.

[53] E. V Lavrov, F. Herklotz, J. Weber, Identification of two hydrogen donors in ZnO, Phys. Rev. B. **79**, 165210 (2009). https://doi.org/10.1103/PhysRevB.79.165210.

[54] R. Peter, K. Salamon, A. Omerzu, J. Grenzer, I.J. Badovinac, I. Saric, M. Petravic, Role of Hydrogen-Related Defects in Photocatalytic Activity of ZnO Films Grown by Atomic Layer Deposition, J. Phys. Chem. C. **124**, 8868 (2020). https://doi.org/10.1021/acs.jpcc.0c01519.

[55] S. Lautenschlaeger, S. Eisermann, G. Haas, E.A. Zolnowski, M.N. Hofmann, A. Laufer, M. Pinnisch, B.K. Meyer, M.R. Wagner, J.S. Reparaz, G. Callsen, A. Hoffmann, A. Chernikov, S. Chatterjee, V. Bornwasser, M. Koch, Optical signatures of nitrogen acceptors in ZnO, Phys. Rev. B. **85**, 235204 (2012). https://doi.org/10.1103/PhysRevB.85.235204.

[56] J.W. Sun, Y.M. Lu, Y.C. Liu, D.Z. Shen, Z.Z. Zhang, B. Yao, B.H. Li, J.Y. Zhang, D.X. Zhao, X.W. Fan, Nitrogen-related recombination mechanisms in p-type ZnO films grown by plasma-assisted molecular beam epitaxy, J. Appl. Phys. **102**, 43522 (2007). https://doi.org/10.1063/1.2772581.

[57] S. Lautenschlaeger, S. Eisermann, B.K. Meyer, G. Callison, M.R. Wagner, A. Hoffmann, Nitrogen incorporation in homoepitaxial ZnO CVD epilayers, Phys. Status Solidi – Rapid Res. Lett. **3**, 16 (2009). https://doi.org/https://doi.org/10.1002/pssr.200802215.

[58] S.J. Jokela, M.D. McCluskey, Unambiguous identification of nitrogen-hydrogen complexes in ZnO, Phys. Rev. B. **76**, 193201 (2007). https://doi.org/10.1103/PhysRevB.76.193201.

[59] J. Villafuerte, O. Chaix-Pluchery, J. Kioseoglou, F. Donatini, E. Sarigiannidou, J. Pernot, V. Consonni, Engineering nitrogen- and hydrogen-related defects in ZnO nanowires using thermal annealing, Phys. Rev. Mater. **5**, 056001 (2021). https://doi.org/10.1103/PhysRevMaterials.5.056001.